Measurements of Cavitation Dose, Echogenicity, and Temperature during Ultrasound Ablation

T. Douglas Mast, Vasant A. Salgaonkar, Chandrapriya Karunakaran, John A. Besse, Saurabh Datta, and Christy K. Holland

Department of Biomedical Engineering, University of Cincinnati, Cincinnati, Ohio 45267-0586

Abstract. Ultrasound ablation experiments were performed, with simultaneous measurements of acoustic emissions, tissue echogenicity, and tissue temperature, on fresh, degassed bovine liver. The tissue was exposed to bursts of unfocused, continuous-wave, 3.10 MHz from a 3 mm-diameter, 32-element array, which performed B-scan imaging with the same piezoelectric elements during quiescent periods. Exposures employed pulse lengths of 0.9–3.3 s with pressure amplitudes of 0.8–1.4 MPa and duty cycles of 97–99% for exposure times of 6–20 min, sufficient to achieve significant thermal coagulation in all cases. RF echo traces from the array, time-domain signals received by a 1 MHz, unfocused passive cavitation detector, and tissue temperature detected by a needle thermocouple were sampled 0.3–1.1 times per second. Tissue echogenicity was quantified, within the region of significant tissue heating, from the amplitude of RF signals received by the array. Cavitation dose was quantified from the spectra of signals measured by the passive cavitation detector, including subharmonic signal components at 1.55 MHz, broadband signal components within the band 0.3–1.1 MHz, and low-frequency components within the band 10–30 kHz. Tissue ablation effects were assessed by quantitative analysis of digitally imaged, macroscopic tissue sections. Correlation analysis was performed among the averaged and time-dependent acoustic emissions in each band considered, tissue echogenicity, tissue temperature, and ablation rate. Tissue echogenicity correlated significantly with subharmonic and low-frequency emissions as well as tissue temperature, but was uncorrelated with broadband emissions. Ablation rate correlated significantly with broadband and low-frequency emissions, but was uncorrelated with subharmonic emissions.

Keywords: Intense ultrasound, ablation, therapy monitoring, passive cavitation detection
PACS: 43.80.Sh, 43.35.Ei

INTRODUCTION

The objective of the experiments reported here was to gain understanding of the possible role of cavitation and other gas activity during continuous-wave sonications by unfocused ultrasound. This approach to ultrasound ablation, which has recently been developed and employed by several investigators [1]–[4], has the potential to treat large tissue volumes at rates comparable to radiofrequency ablation and other bulk ablation modalities. As with other thermal ablation methods, noninvasive monitoring and control of energy delivery, tissue temperature, and coagulation effects would improve efficacy.

Cavitation and other gas activity is known to occur during ablation by high-intensity focused ultrasound. Such activity can be exploited to visualize ablation effects [5] or to enhance tissue absorption [6, 7], but can also complicate ultrasound energy deposition and the resulting spatial pattern of tissue coagulation [8]–[10]. Here, acoustic emissions associated with cavitation and other gas activity were passively detected during *in vitro* ultrasound ablation under lower-intensity exposure conditions similar to those reported

CP911, 6th *International Symposium on Therapeutic Ultrasound*
edited by C.-C. Coussios and G. ter Haar

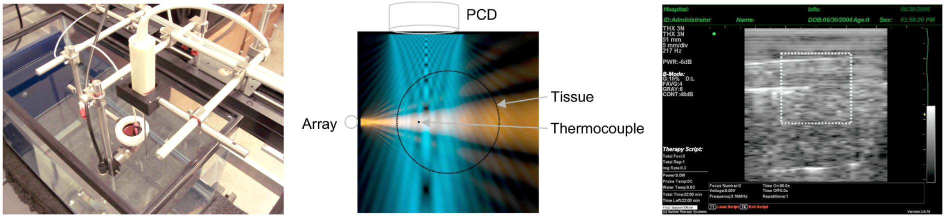

FIGURE 1. Experiment configuration. Left: experimental setup. Middle: top view showing beam of image-ablate array (horizontal) [11], sensitivity pattern of detector at 1 MHz (vertical) [12], and relative positions of the transducers, thermocouple, and tissue. Right: B-scan from the image-treat array showing the region of interest employed for grayscale analysis. The thermocouple tip is seen at the ROI center.

in Ref. [4]. These measurements were intended to clarify the possible roles of cavitation and other gas activity in this treatment regime, including the relationship between gas activity and tissue echogenicity, the effect of gas activity on the progress of thermal ablation, and the possibility of therapy monitoring using passive cavitation detection.

MEASUREMENTS

The experimental configuration employed is shown in Fig. 1. *Ex vivo* bovine liver, less than 12 hours *post mortem*, was freshly cut to dimensions $7 \times 3.5 \times 3$ cm^3 with the liver capsule comprising one of the 7×3.5 cm^2 surfaces. The cut tissue was placed in a latex condom (Probe Guard, Carter-Williams) with a small amount of degassed phosphate-buffered saline, and suspended in a water tank filled with deionized water, with care taken to minimize gas entrainment during tissue handling. Thermal ablation and B-scan imaging were performed using a miniaturized 32-element image-ablate array [4] (THX 3N, Guided Therapy Systems, Mesa, Arizona) with an active surface of 2.3×49 mm^2, placed parallel to the liver capsule at a 10–15 mm distance. Passive cavitation detection was performed using a 25 mm circular diameter, unfocused, 1 MHz broadband receiver (C302, Panametrics), placed perpendicular to the image-ablate array at a distance of 10–15 mm from the opposing tissue surface. A 0.4 mm diameter needle thermocouple (Ella CS type B) was inserted at a depth of 7–8 mm from the tissue surface facing the array, aligned with the array axis. The right panel of Fig. 1 shows a representative B-scan image of the liver tissue sample with the inserted needle thermocouple, obtained using the Iris imaging and ablation system (Guided Therapy Systems, Mesa, Arizona).

Ablation exposures, specified and controlled using the Iris system, were performed by firing the center 16 array elements at 3.1 MHz as an unfocused 2.3×24.5 mm^2 aperture, with amplitudes corresponding to measured acoustic power output of 16.2, 28.8, and 45.0 W. *In situ* acoustic pressure and intensity levels were estimated by computing the diffracted acoustic field of this aperture using a Fresnel approximation [11]. At a distance of 15 mm from the array, the acoustic pressure amplitudes employed were estimated as 0.83, 1.10, and 1.38 MPa (acoustic intensities 23, 41, and 64 W/cm^2). A total of six exposures were performed for each amplitude condition, for a total of 18 experiments.

Exposure times employed, found to ensure significant thermal coagulation in each case, were 20 min for the 0.83 MPa amplitude, 10 min for the 1.10 MPa amplitude, and

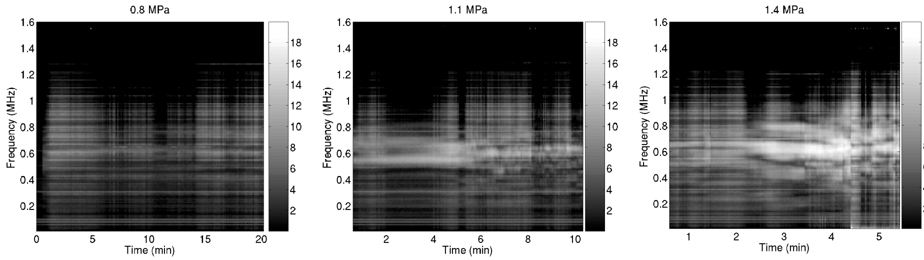

FIGURE 2. Time-frequency plots for representative passive cavitation detector (PCD) spectra at the three exposure conditions employed. Spectra are shown in dB relative to a measured noise level.

5 min for the 1.38 MPa amplitude. Ultrasound exposure was continuous throughout these treatment cycles except for brief interruptions to record B-scan images using the same array, resulting in effective duty cycles of 97–99%. RF echo traces were recorded for each B-scan at a 33 MHz sampling rate using a PC-based A/D card (Compuscope CS 14200, Gage Applied). Signals from the passive cavitation detector (PCD) were recorded at a 10 MHz sampling rate for 100 ms intervals synchronized to begin 100 ms after image acquisition, ensuring that these signals were recorded during a steady state of the continuous-wave exposure. These signals were recorded at intervals respectively corresponding to 0.3, 0.6, and 1.1 acquisitions per second for the 0.83, 1.11, and 1.38 MPa amplitudes. Temperature from the needle thermocouple probe was recorded using a digital data logger (Omegaette HH306, Omega Inc.) and recorded temperatures were temporally interpolated to correspond with the sampling times of the echo trace and PCD signal acquisitions.

After each ablation treatment, tissue samples were frozen and sectioned into calibrated macroscopic slices of 2 mm thickness for evaluation [4]. Areas ablated in each tissue section were quantified by manual segmentation based on gross discoloration (ImageJ, National Institutes of Health). The total treated volume was thus estimated and employed to compute volumetric ablation rates (ml/min) for each experiment, which respectively averaged 0.14, 0.66, and 1.15 ml/min for the 0.83, 1.11, and 1.38 MPa amplitudes.

DATA PROCESSING

Acoustic emissions, intended to quantify cavitation and other gas activity, were quantified by spectral analysis of PCD signals. For each 100 ms signal, a power spectrum density was estimated by the periodogram method using 1000-sample rectangular windows with no overlap, so that 1000 periodograms (magnitude-squared discrete Fourier transforms) were averaged to obtain each power spectrum. Representative time-frequency plots of these spectra for each exposure condition are shown in Fig. 2. To isolate different physical mechanisms of gas activity, spectral energy was integrated within three frequency bands. The first band considered, consisting of the single frequency bin centered at the subharmonic frequency of 1.55 MHz, is sensitive to nonlinear bubble vibrations sometimes associated with stable cavitation activity [13]. The second band, covering frequencies 0.3–1.1 MHz, was chosen to characterize broadband emissions such as those resulting from inertial bubble collapse [13]. The third, ranging from 10–30 kHz,

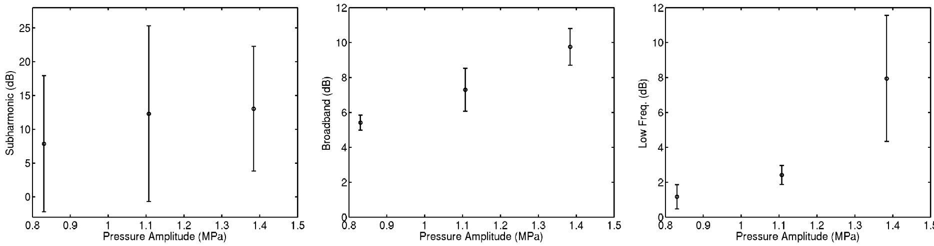

FIGURE 3. Average PCD spectrum levels within subharmonic, broadband, and low-frequency intervals at the three exposure conditions employed. Plotted are the mean and standard deviation for each case ($N = 6$).

characterizes low-frequency emissions associated with tissue boiling [14]. Time-average spectral energy was also computed in these bands for each experiment and quantified in dB relative to the measured noise floor, providing a "cavitation dose" for each band.

The time variation of tissue echogenicity was calculated using the RF echo data recorded from the image-ablate array. For each measurement, echo energy was quantified as the mean-square value of the echo signals within a region of interest spanning 24.5 mm or 16 lines in azimuth (corresponding to the extent of the therapy beam), and from 8–32 mm in range (the region predominantly heated by the therapy beam, approximately centered on the active thermocouple element). Because the initial echogenicity varied from sample to sample depending on the tissue structure, mean grayscale values were computed in dB relative to the mean value at the beginning of treatment.

Possible artifacts in the measured acoustic emissions were controlled for in several ways. First, it was confirmed that the 1 MHz PCD successfully recorded broadband emissions within the frequency range 0.3–1.1 MHz during acoustic destruction of an ultrasound contrast agent (Optison, Amersham Health), in a manner similar to the low-frequency passive cavitation detection performed in Ref. [15]. The influence of electronic interference was assessed by performing the same data acquisition while driving a 50 Ω transducer-mimicking load at 3.1 MHz by the Iris system at the highest amplitude considered. The resulting spectra, which were indistinguishable from spectra measured in the absence of any signal, were used as reference values for computation of the time-averaged emissions. In addition, to control for possible thermocouple artifacts, two measurements were performed at each amplitude condition without the needle thermocouple. It was found that comparable acoustic emissions occurred in the absence of the thermocouple, so that any cavitation seeding caused by the thermocouple needle was of secondary importance for the analyzed experiments.

Correlation analyses were performed among the time-averaged and instantaneous measured quantities. The ablation rate for each experiment ($N = 18$) was correlated to the average subharmonic, broadband, and low-frequency acoustic emission level. In addition, all time-dependent measured quantities, including tissue temperature, mean grayscale value, and acoustic emissions in the three bands considered, were cross-correlated for all temporal epochs recorded ($N = 6179$ for all data points in the 18 experiments). Correlation coefficients were computed for each possible pair of variables, and corresponding p-values were computed to assess statistical significance.

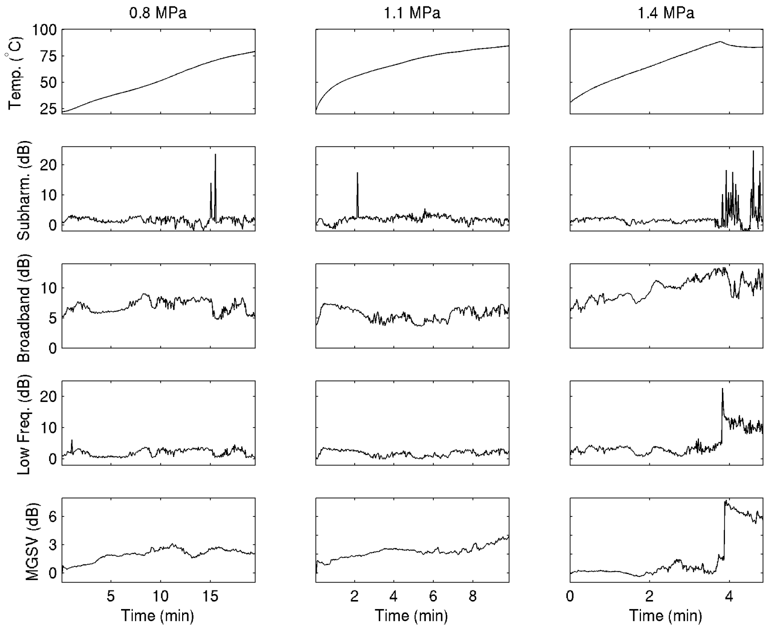

FIGURE 4. Representative plots of the measured time-dependent variables for each of the three exposure conditions employed.

RESULTS

Mean and standard deviation values for the time-averaged acoustic emission levels, based on measured spectra for all 18 experiments analyzed, are shown in Fig. 3 for the three frequency bands considered. Emissions at the subharmonic frequency were found to be vary across experiments, consistent with the large standard deviations shown (comparable to the mean emission level in each case). Broadband emissions were much more consistent, with time-averaged levels that predictably increased with the exposure pressure amplitude, and relatively small deviations between experiments. Low-frequency emissions were generally small for the 0.83 MPa and 1.10 MPa amplitudes, but larger and more variable for the 1.38 MPa amplitude. This is consistent with the expectation that tissue boiling is more likely to occur at higher acoustic intensities.

Representative time series for experiments at each exposure condition are shown in Fig. 4, for the same experiments illustrated in Fig. 2. The temperature time history shows a significant rise over the course of each experiment to temperatures $> 75°C$ associated with significant thermal ablation, with higher heating rates at higher acoustic amplitude as expected. The decline in slope about 4 min into the highest-amplitude treatment is consistent with acoustic shadowing caused by tissue vaporization proximal to the thermocouple [10]. Subharmonic emissions occur in each case shown, appearing sporadically at the two lower amplitudes but late in the highest-amplitude treatment, after the apparent tissue vaporization. Broadband emissions are largest in the highest-

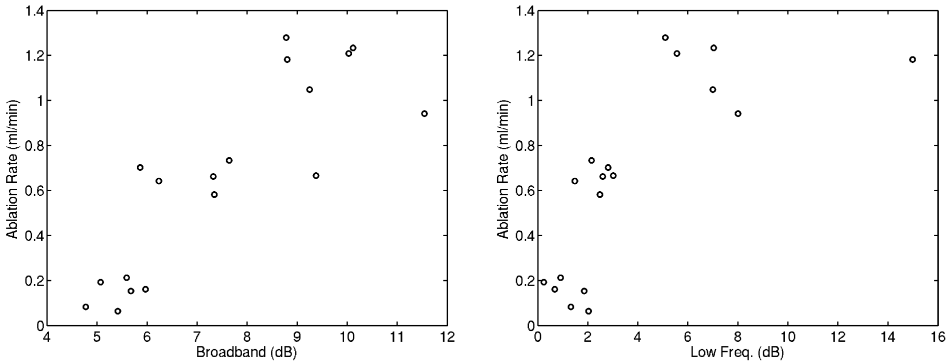

FIGURE 5. Scatter plots of ablation rate vs. average acoustic emission levels for the broadband and low-frequency intervals considered. Points are shown for 18 experiments at the three exposure conditions employed.

amplitude case, and increase with temperature to a limited extent. Low-frequency emissions are small except in the highest-amplitude case after the apparent vaporization. Tissue echogenicity rises with temperature to a limited extent, except in the highest-amplitude case where a rapid increase occurs at the time of apparent tissue vaporization.

Time-averaged levels for broadband and low-frequency emissions correlated strongly with ablation rate across the 18 experiments analyzed, as illustrated in Fig. 5, but did not correlate significantly with subharmonic emissions. Correlation coefficients computed with the tissue ablation rate were $r = 0.144$ ($p = 0.569$) for the subharmonic emissions, $r = 0.848$ ($p = 8.64 \cdot 10^{-6}$) for the broadband emissions, and $r = 0.747$ ($p = 3.70 \cdot 10^{-4}$) for the subharmonic emissions. The scatter plots shown in Fig. 5 suggest that ablation rate is correlated approximately linearly with broadband emissions but nonlinearly with low-frequency emissions. The latter observation suggests a consistency between tissue vaporization and rapid volume ablation, both of which are associated with rapid temperature rises in the experiments considered.

The correlation matrix for all time-dependent variables measured is shown in Table 1, with statistically significant correlations indicated in bold type. Temperature is seen to correlate significantly with low-frequency emissions, broadband emissions, and relative tissue echogenicity (mean grayscale value), with low-frequency acoustic emissions showing the strongest correlation. The relative grayscale value correlates significantly with low-frequency and subharmonic emissions, although the measured correlation coefficients are relatively low (< 0.25). Tissue echogenicity was not significantly correlated with broadband emissions in these experiments.

CONCLUSIONS

Measurements of acoustic emissions, temperature, and tissue echogenicity during ultrasound ablation experiments allow the role of gas acitivity to be assessed. The results indicate that, for the exposure conditions studied, subharmonic emissions are not a consistent indicator of ablation-relevant bubble activity, but that broadband emissions

TABLE 1. Correlation matrix for time-dependent quantities over all measured epochs ($N = 6179$ for the 18 experiments). Correlation coefficients in bold type are statistically significant ($p < 10^{-25}$ in all cases).

Subharmonic	Broadband	Low-frequency	Grayscale	
$-3.39 \cdot 10^{-3}$	**0.433**	**0.529**	**0.436**	Temperature
	$1.02 \cdot 10^{-4}$	$3.54 \cdot 10^{-3}$	**0.123**	Subharmonic
		0.651	$2.32 \cdot 10^{-3}$	Broadband
			0.218	Low-frequency

increase proportionately to the acoustic pressure amplitude and ablation rate, while low-frequency emissions are strongly associated with tissue vaporization and boiling. Thus, broadband and low-frequency emissions from tissue, together with tissue echogenicity and other image-based measurements, may be useful for noninvasive monitoring of energy delivery and tissue state during ultrasound ablation treatments.

REFERENCES

1. C. J. Diederich, W. H. Nau, and P. R. Stauffer, "Ultrasound applicators for interstitial thermal coagulation," IEEE Trans. Ultras., Ferroelect., Freq. Contr. **46**, 1218–1228 (1999).
2. R. Chopra, C. Luginbuhl, A. J. Weymouth, F. S. Foster, and M. J. Bronskill, "Interstitial ultrasound heating applicator for MR-guided thermal therapy," Phys. Med. Biol. **46**, 3133–3145 (2001).
3. F. Prat, C. Lafon, D. M. de Lima, Y. Theilliere, J. Fritsch, G. Pelletier, C. Buffet, an d D. Cathignol, "Endoscopic treatment of cholangiocarcinoma and carcinoma of the duodenal papilla by intraductal high-intensity US: Results of a pilot study," Gastrointest. Endosc. **56**:909–915 (2002).
4. I. R. S. Makin, T. D. Mast, W. Faidi, M. M. Runk, P. G. Barthe, and M. H. Slayton, "Miniaturized ultrasound arrays for interstitial ablation and imaging," Ultras. Med. Biol. **31**, 1539–1550 (2005).
5. B. A. Rabkin, V. Zderic, and S. Vaezy, "HIFU-induced hyperecho in ultrasound images, cavitation activity and thermal behavior," *4th International Symposium on Therapeutic Ultrasound* (American Institute of Physics Proceedings CP754), pp. 43–46 (2004).
6. R. G. Holt and R. A. Roy, "Measurements of bubble-enhanced heating from focused, MHz-frequency ultrasound in a tissue-mimicking material," Ultrasound Med. Biol. **27**, 1399–1412 (2001).
7. S. D. Sokka, R. King, and K. Hynynen, "MRI-guided gas bubble enhanced ultrasound heating in *in vivo* rabbit thigh," Phys. Med. Biol. **48**, 223–241 (2003);
8. N. A. Watkin, G. R. ter Haar, and I. Rivens, "The intensity dependence of the site of maximal energy deposition in focused ultrasound surgery," Ultras. Med. Biol. **22**, 483–491 (1996).
9. W.-S. Chen, C. Lafon, T. J. Matula, S. Vaezy, and L. A. Crum, "Mechanisms of lesion formation in high intensity focused ultrasound therapy," Acoust. Res. Lett. Online **4**, 41–46 (2003).
10. T. D. Mast, I. R. S., Makin, W. Faidi, M. M. Runk, P. G. Barthe, and M. H. Slayton, "Bulk ablation of soft tissue with intense ultrasound: modeling and experiments," J. Acoust. Soc. Am. **118**, 2715–2724 (2005).
11. T. D. Mast, "Fresnel approximations for ultrasonic fields of rectangularly symmetric sources," IEEE Trans. Ultrason., Ferroelect., Freq. Contr., submitted (2006).
12. T. D. Mast and F. Yu, "Simplified expansions for radiation from a baffled circular pi ston," J. Acoust. Soc. Am. **118**, 3457–3464 (2005).
13. X. Yang and C. C. Church, "Nonlinear dynamics of gas bubbles in viscoelastic media," Acoust. Res. Lett. Online **6**, 151–156 (2005).
14. S. P. Ying, J. E. Knight, and C. C. Scott, "Background noise for acoustic emission in boiling water and a pressurized water nuclear-power reactor," J. Acoust. Soc. Am. **53**, 1627–1631 (1973).
15. T. Giesecke and K. Hynynen, "Ultrasound-mediated cavitation thresholds of liquid perfluorocarbon droplets *in vitro*," Ultrasound Med. Biol. **29**, 1359–1365 (2003).